CRYSTAL GROWTH & DESIGN

pubs.acs.org/crystal

Article

Projected Cost of Gallium Oxide Wafers from Edge-Defined Film-Fed Crystal Growth

Karen N. Heinselman,* Drew Haven, Andriy Zakutayev, and Samantha B. Reese*

Cite This: *Cryst. Growth Des.* 2022, 22, 4854−4863

Read Online

ACCESS | Metrics & More | Article Recommendations

ABSTRACT: Gallium oxide (Ga_2O_3) is an emerging ultra-wide bandgap semiconductor that has unique properties ideal for high-power, high-temperature, optoelectronic, and sensing applications and has piqued interest over the last decade. It has the potential to be technologically and economically superior to commercially available wide bandgap semiconductor materials, such as silicon carbide and gallium nitride, because its wider bandgap enables increased breakdown voltages and lower on-state resistances, and its ability to be grown from melt enable cost-competitive economics. In this study, we present a techno-economic analysis that projects the cost of 6″ β-Ga_2O_3 wafers fabricated from crystals grown via edge-defined film-fed growth (EFG). At a manufacturing volume of 5000 wafers per month, we predict a unit cost of $320 for a 6″ EFG grown β-Ga_2O_3 epi-wafer. We determine that, when calculated using 2021 iridium crucible costs, EFG has a 2× cost advantage compared to previously reported epi-wafers grown via the Czochralski (CZ) method. We further identify key cost parameters for 6″ β-Ga_2O_3 epi-wafers and present cost-sensitivity analysis of their impact on the final cost.

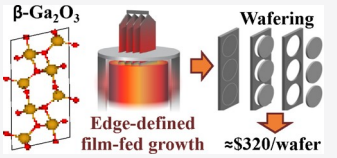

1. INTRODUCTION

Ultra-wide bandgap electronics based on gallium oxide (Ga_2O_3) have the potential to outcompete wide bandgap silicon carbide (SiC) and gallium nitride (GaN) in both performance[1] and cost.[2] The monoclinic β-Ga_2O_3 phase (which is the stable phase at ambient conditions and will be the phase referred to as Ga_2O_3 throughout this discussion) can be grown using common melt-growth methods,[3] reducing the cost per wafer significantly relative to GaN and SiC. Despite its lower mobility and thermal conductivity relative to SiC, Ga_2O_3 has a wider bandgap, leading to increases in breakdown voltages and reduced on-state resistances, both of which are favorable for power electronics.[4] Other promising applications include communications, flame detection, photolithography, and solar-blind UV detectors (cutoff wavelength < 280 nm),[3,5,6] which enable the detection of very weak short-wavelength signals.[7−9] Additionally, Ga_2O_3 performs well in the high-temperature application space,[10−12] in which lower thermal conductivity and mobility are less of a detriment than in more conventional operational environments. There is significant interest in, and corresponding research into, reliable high-temperature Ga_2O_3-based electronics, including Schottky diodes[11,12] and sensors.[13−15]

A variety of different melt-growth techniques are used to grow large single crystals of oxides for electronics. Ga_2O_3[3,16] is no exception and has been grown using edge-defined film-fed growth (EFG),[17,18] Czochralski (CZ) growth,[19−21] Kyropoulos, vertical Bridgman technique,[22] and variations on these melt-growth techniques. Among these methods, EFG and CZ have shown promise for the bulk growth of Ga_2O_3. However, the unique properties of gallium oxide present issues for scaling up of boules to larger diameters. One such property is thermal conductivity. As a comparison, thermal modeling of CZ-grown sapphire (Al_2O_3) boules has been performed by several groups to better understand the effects of thermal profiles and built-up thermal stresses.[23−26] Experimentally, in CZ-grown Al_2O_3 boules, the thermal stresses remain the limiting factor, prohibiting defect-free crystal growth beyond a diameter of around 4″ to 5″.[27] Ga_2O_3 has a lower thermal conductivity than Al_2O_3, which further limits the feasibility of three-dimensional Ga_2O_3 melt growth. This limitation renders the growth of 6″ diameter boules infeasible from a practical standpoint.[16,28]

Fortunately, we can reduce the effective dimensionality during growth to two dimensions by growing EFG ribbons, as shown in Figure 1 (top). In both the EFG and CZ growth methods, precursor powder is loaded into the crucible and inductively heated to a melt. For both methods, a seed crystal (or multiple, when scaling up EFG) is then dipped down to touch the melt, initiating crystal growth and encouraging grain propagation to template off the seed crystal. The seed is then pulled up and through the hot zone as the material crystallizes. In EFG (Figure 1 top), the crystal is pulled off of a die placed in the melt, and the shape of the resulting crystal is defined by the cross-sectional dimensions of the die.[29,30] A common geometry is a long thin sheet, known as a ribbon.

Received: March 18, 2022
Revised: June 9, 2022
Published: July 5, 2022

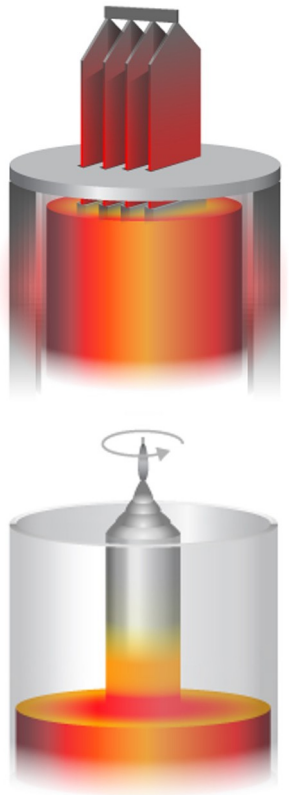

Figure 1. Pulling wafers from a melt via (Top) edge-defined film-fed growth method for pulling ribbons and (Bottom) the Czochralski method for pulling boules.

Comparatively, in CZ (Figure 1 bottom), the seed crystal is pulled up and simultaneously rotated to (ideally) form a consistent cylindrical crystal.[26,31,32] Pulling ribbons from the melt at a thickness of 1−3 mm, as shown in Figure 1 (top), solves much of the thermal management problem and allows for a more facile path forward.[33] EFG growth has been done successfully for both sapphire[27,29,34] and Ga_2O_3[17,18] single-crystal wafers.

The importance of techno-economic analysis (TEA) becomes clear when considering the scale-up of technologies for commercial electronics. Economic viability is a large driving factor for the adoption of electronics and energy generation technologies.[35−40] For instance, the use of SiC increases the manufacturing price of a photovoltaic (PV) inverter; however, the improvements in performance ultimately result in a lower cost of energy generation.[39] Additionally, SiC power modules are more expensive than Si-based modules; however, the SiC enabled design enhancements render the manufactured cost of medium-voltage variable-frequency motor drives on par with their Si counterparts.[40] These are excellent examples demonstrating how TEA can analytically quantify scale-up potential. In both examples, the upstream cost was higher than the state-of-the-art, but TEA was able to demonstrate the final energy technology product still had favorable economics.[39,40] TEA can also be used upstream at the manufacturing level to demonstrate the potential for a technology to be transformative. It has been used extensively in understanding Si PV manufacturing to identify critical innovation areas and outline routes that allow Si PV to meet cost targets.[37] TEA can also be used to break down the cost of non-commercialized technologies to understand if scaling is feasible. It was used to demonstrate that even though the substrate is the cost driver for III-V solar cells, substrate reuse offers only limited cost reduction potential because of the increased preparation costs.[38] We presented an initial TEA of 6″ Ga_2O_3 epi-wafers grown via the CZ method in 2019.[2] Two main findings were of particular interest in the previous TEA paper. First, the cheaper and softer Ga_2O_3 material enables it to be less expensive than the state-of-the-art SiC used for power electronics. Second, the cost of the crucible was a major factor in the total cost per Ga_2O_3 wafer.

In this study, we present a feasibility and cost-comparison analysis of Ga_2O_3 grown via EFG to reflect the current knowledge of substrate manufacturing and the engineering limitations thereof. The thermal limitations mentioned above make growth of Ga_2O_3 wafers comparable in size to SiC wafers via CZ infeasible. In both CZ and EFG, the crucible cost was found to be a major contributing factor to the total cost of the wafers. Using the current iridium prices, the CZ model has a significantly increased cost per wafer, as EFG growth methodology allows for a reduction in the required crucible size. Ultimately, the total cost per Ga_2O_3 epi-wafer, grown via EFG, was found to be ∼$320 as compared to ∼$620 for CZ grown wafers using 2021 iridium crucible pricing. We also performed cost-sensitivity analysis to determine the effects that crucible price and reuse, as well as crystal growth rates and thicknesses, have on the final Ga_2O_3 per-wafer costs.

2. METHODS

To determine the cost of Ga_2O_3 wafers, a bottom-up cost model was created to account for growing substrates via EFG, which was then compared to the previous CZ growth model, updated to reflect current iridium pricing. The modeled steps for the EFG process flow are shown in Figure 2. These steps consist of crucible procurement, crystal growth, reshaping/coring, grinding/lapping, surface prepara-

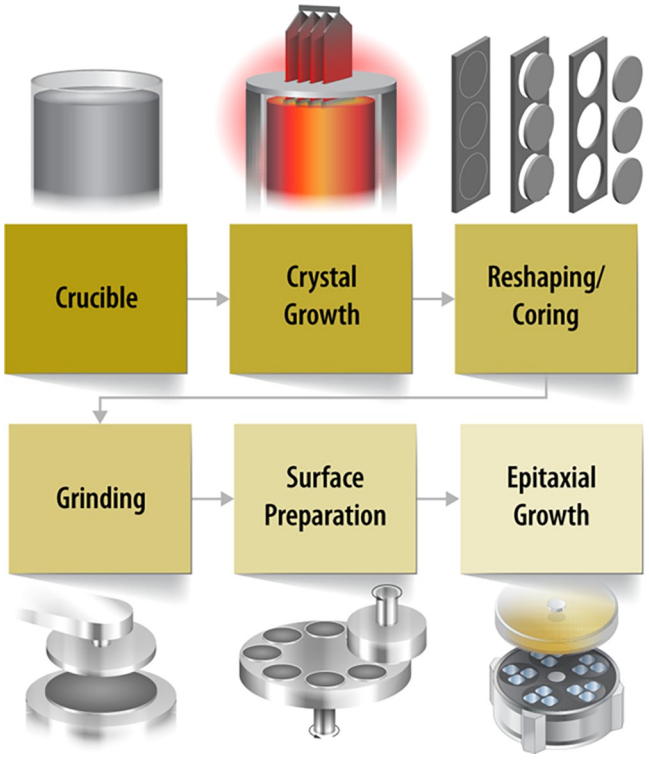

Figure 2. Process flow for the EFG growth of Ga_2O_3.

https://doi.org/10.1021/acs.cgd.2c00340
Cryst. Growth Des. 2022, 22, 4854−4863

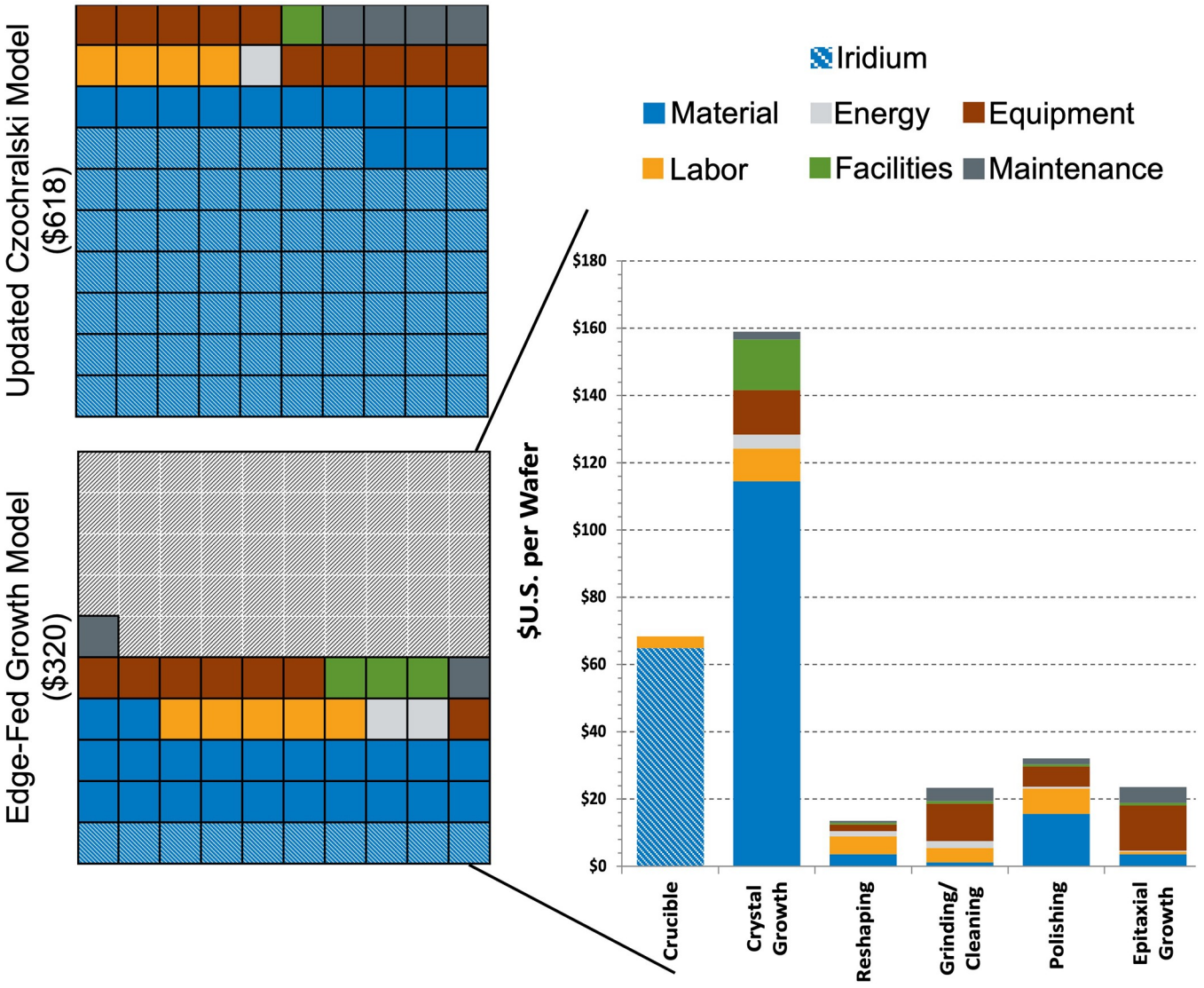

Figure 3. (Left) Cost comparison between EFG and CZ growth methods using 2021 Iridium prices. (Right) Wafer cost breakdown of EFG-grown Ga_2O_3. All costs are *per wafer*, including "crucible," which is the cost of the Ir crucible *per wafer*, accounting for the dramatic increase in iridium prices.

tion (which includes polishing and wafer cleaning), and epitaxial growth. As in the previous work,[2] the equipment and facility were assumed to be new and dedicated only to this process.

Input parameters for the model, including labor requirements, building space, equipment cost, cycle times, material and utility usage, and maintenance, were collected from discussion with industry members and literature surveys. The linear depreciation times for equipment and building lifetimes were as those set in the previous work,[2] with the equipment lifetime set at 7 years and the building lifetimes at 20 years. In the new model, the reshaping/coring step is used to create the shape of the wafers; 6″ circular wafers were cut out of the long, flat ribbon grown via EFG. The grinding step is needed to thin the wafers down to appropriate thickness and to eliminate any bubbles or defects that may form on the as-grown ribbon's surface.

3. RESULTS

The main results of this TEA study are summarized in Figure 3, which shows the breakdown of the cost per expense category for each of the six manufacturing steps. As shown in Figure 3 (right), the two major cost contributions of the Ga_2O_3 wafers manufactured from the EFG crystal growth process are the cost of the crucible and the cost of the high-purity Ga_2O_3 powder (which is the majority of the material cost in the "crystal growth" step). In comparing the previous CZ model to the current EFG model (Figure 3, left), the largest differences in cost are the crucible price (higher for CZ) and the amount of Ga_2O_3 powder that is consumed (higher for EFG).

Iridium has experienced a roughly 6× increase in price (discussed in section 4.1) since the completion of the previous CZ-based model. Thus, to allow for a better comparison between growth methods, the CZ model was re-run, changing only the crucible price to reflect the current 2021 iridium valuation. Figure 3 (left) shows the resulting comparison. The iridium price increase translated into a CZ per-wafer cost increase from the previously reported $283 to $618. This demonstrates that EFG growth results in a nearly 2× cheaper Ga_2O_3 wafer than a CZ-grown Ga_2O_3 wafer at today's iridium prices. Material costs drive the overall EFG wafer manufacturing cost. Figure 3 (right) shows that the crucible and the Ga_2O_3 powder costs account for over 88% of material costs and greater than 55% of manufacturing cost. Adding in materials costs, such as the grinding pads, gases, polishing

https://doi.org/10.1021/acs.cgd.2c00340
Cryst. Growth Des. 2022, 22, 4854−4863

wheels, and so forth, brings material cost contributions to about 2/3 of total manufacturing cost. The next significant contributor is the equipment, which constitutes 14% of the cost. Decreasing the time necessary to polish or increasing the pull rate for the crystal growth would reduce equipment cost. Growing ribbons closer to final wafer dimensions would additionally reduce material and equipment costs. The cumulative yield loss is assumed to be just over 40%, so yield loss reductions would result in additional cost savings. The total EFG-grown wafer cost, shown on the left in Figure 3, was calculated to be $320 as compared to the $283 previously reported for CZ-based growth.[2]

Below, we discuss each manufacturing step and the key differences between the CZ and EFG crystal growth processes, and the effects that those have on the cost models presented in Figure 3.

3.1. Crucible. In this EFG TEA model, crucible procurement is broken out separately because it is such a significant portion of the total cost and reflects the direct iridium costs. The Ga_2O_3 powder is accounted for in the crystal growth stage of the model. This better allows researchers to see the individual effects of the two large material contributions to the overall costs. It highlights the effects that advances in crucible technology, discussed later, or increased adoption of Ga_2O_3 (which would lead to further Ga_2O_3 powder cost reductions due to economies of scale), would have on the overall wafer manufacturing cost.

The cost of iridium, which is used as the crucible material for Ga_2O_3 growth, has increased significantly over the past 5 years. When switching from CZ to EFG, the crucible size can be reduced. In this scenario, a stable continuous growth would be achieved without interruption by feeding additional Ga_2O_3 powder into the crucible during growth. This is enabled by the thermal isolation of the solid−liquid growth interface from the melt reservoir, which is provided by the capillary rise of melt through the die in the EFG process.[33,34] Additionally, in EFG growth the crucible can be grown empty; whereas in CZ a significant portion of the melt (approx. 50%) cannot be crystallized and remains in the crucible. This difference alone accounts for a reduction in crucible volume of up to 50% for a comparable crystallized volume. The reduced crucible size reduces the amount of expensive iridium needed, which significantly reduces the crucible cost. The model assumes that 80% of the raw iridium material cost can be recovered through recycling when the crucible reaches end of life. The model further assumes a 4× longer crucible life compared to that presented in 2019, as the lower oxygen content required in Ga_2O_3 EFG growth does not degrade the crucible as much as the higher O_2 (or CO_2) partial pressures needed for CZ,[41] thus increasing EFG crucible lifetimes. Furthermore, the literature indicates a large difference in the thermal expansion coefficients causes crucible degradation.[31,42] The abilty of the EFG crucible to be grown empty also enables faster growth rates. This makes the crucible less susceptible to wear upon heating and cooling, and reduces damage from melt volatilization, as the material is molten for less time,[21] thus additionally supporting the longer life assumption. Figure 5a shows wafer price sensitivity to crucible reuse.

To calculate the crucible cost, the dimensions of the crucible needed were first considered, specifically to accommodate the wafer width and the target number of 16 ribbons pulled at a time. Each ribbon was taken to be 155 mm wide (6″ plus a couple of millimeters to account for the reshaping step) and 1.5 mm thick (which is set by the die slot size). The crucible inner diameter was thus assumed to be 200 mm wide, and the wall thickness was kept as small as possible. One added advantage of EFG growth, at least when the crucibles are prohibitively expensive, is the ability to perform continuous-fed growth, so the crucible was assumed to be just under 80 mm tall. From these dimensions, the physical volume of the crucible material needed was calculated and translated to a total crucible weight, and the cost of iridium in March 2021 ($6000/troy oz) was used to give the total material cost. Using the Design for Manufacture and Assembly (DFMA) software,[43] an additional machining cost of 5% of the material cost was included in the total crucible cost. Based on these parameters, even with minimizing the amount of iridium used, the cost comes to over $1.3 million per crucible.

This $1.3 million crucible cost is divided over the number of wafers grown during an assumed 40-run lifetime. At end of life, an 80% iridium material buyback for recycling the crucible and die was assumed, bringing the actual crucible cost to $257,000. This recycling step significantly reduces the cost per wafer. Even so, the cost of the crucible material alone accounts for over $60 of the total cost per wafer, as shown in Figure 3a, when we also include the cumulative yield loss of 40%. The total labor cost for the crucible step added less than $5 to the total wafer cost, in comparison, for a total of under $70/wafer for crucible procurement.

3.2. Crystal Growth. When transitioning from CZ to EFG, there is an increase in the amount of Ga_2O_3 powder consumed. For EFG, the excess material cut off during the coring/reshaping step can be reclaimed by grinding it up and feeding it back into the crucible for the next growth. This reduces the material disparity between CZ and EFG; however, the EFG-grown wafer must also be ground and polished down to achieve the targeted wafer thickness and to produce good quality surfaces free of bubbles, warping, and so forth. Material removed during the grinding/polishing process step is assumed to be nonrecoverable because of contamination from the grinding wheel and grinding/polishing slurries used. Ultimately, the powder used corresponds to the amount of material fed into the crucible, minus the material recovered in the coring/reshaping step. Thus, the model feeds the coring/reshaping step back into the crystal growth step for accuracy. In contrast, the CZ boule is assumed to be grown to the final diameter; thus, less material needs to be removed during the grinding/polishing step, as the surfaces of the wafers are cut, rather than the as-grown outer surface.

One benefit gained from the transition from CZ to EFG is an increase in the achievable growth/pull rate during the crystal growth step. In the CZ growth of silicon, if the pull rate is too fast, boules often exhibit crystal spiraling, which can result in a loss of control over the crystal diameter.[26] There is a wide range of different conditions and triggers for the onset of spiral growth in oxide crystals with high melting points.[44] EFG, on the other hand, allows for a much higher maximum pull rate, although the growth parameters (including pull rate) still can have a significant effect on the resulting oxide crystal.[45] This maximum pull velocity, assuming radiation into absolute zero (a 0 K environment) is given by eq 1, below:[46]

$$(V_g)_{max} = \frac{\sqrt{\sigma \times \varepsilon \times k_m \times T_m^5}}{L \times \sqrt{t}} \quad (1)$$

https://doi.org/10.1021/acs.cgd.2c00340
Cryst. Growth Des. 2022, 22, 4854−4863

where V_g is the growth velocity, L is the latent heat of fusion per unit volume of the solid, ε is the emissivity of the ribbon's surface, k_m is the thermal conductivity of the solid at the melt temperature, T_m is the melt temperature in Kelvin, and t is the thickness of the ribbon being pulled. The Stefan−Boltzmann constant, σ, has a value of 5.67×10^{-8} W/(m^{2}K^4).

Using values found in the literature for numerical analysis of CZ-grown Ga_2O_3, and taking into account the difficulties of growing large-size bulk crystals,[28,42] the latent heat is given to be L = 5792 kJ/kg, the emissivity is ε = 0.3, the melting point is T_m = 1802 °C = 2093 K, and the thermal conductivity of the solid is k_m = 21 W/(m*K). For unit conversion, the density of solid Ga_2O_3 at the melting point is 5945 kg/m^3. The latent heat of the solid can then be converted to L = 9.56E6 W*h/m^3. The maximum pull rate, with some basic unit conversion, comes out to 396 mm$^{3/2}$/h*$t^{-1/2}$. Thus, assuming a 1 mm thick ribbon, the maximum pull rate is around 396 mm/h. As a comparison, the maximum pull rate for a 2-mm-thick ribbon is 280 mm/h. Noting that the pull rate from this calculation is a maximum pull rate, and that it does not account for quality of the resulting crystal, we chose to use 1/10th of the calculated maximum pull rate in the model as a more conservative estimate of the time spent during crystal growth. For the base model, we assumed a pull rate of 30 mm/h, as pull rates of 10 to 15 mm/h have already been demonstrated,[47,48] as well as an as-pulled ribbon thickness of 1.5 mm and a total ribbon length of 2 meters.

For the crystal growth process, the material cost again dominates in the total cost. While there are some minor costs involved for the seed crystal used to template the crystal orientation, as well as the gases to control the growth environment, the driving material cost for this step is the Ga_2O_3 powder. The portion of the ribbon removed when forming circular wafers during the reshaping/coring step is assumed to be ground up and fed back into the crystal growth step to help reduce material costs. The costs of grinding this material for reuse are assumed to be negligible. However, even with the excess precursor material recovery, the material cost, including the precursor powder, gases, and seed crystal, was calculated at around $114/wafer. The total cost of the crystal growth process step was around $159/wafer, which includes the labor, energy, equipment, facilities, and maintenance costs, as well as the materials consumed.

3.3. Reshaping/Coring. In the reshaping/coring step, circular wafers are cut out of the EFG-grown ribbons to enable facile transfer to typical semiconductor wafer manufacture equipment. The material removed in this step is then cleaned, reground, and fed back into the crucible as described above, which reduces the amount of material consumed per wafer. For these material reuse calculations, some variables must be considered: ribbon width (w), ribbon thickness (t), number of ribbons pulled (N), length of the ribbons pulled (l), the wafer diameter cut out of the ribbons (d), and the number of wafers per ribbon (n). Assuming that the initial necking and spreading off from the seed crystal are automatically fed back into the crucible and not used for the wafers, we can effectively ignore that section of the ribbon in these calculations. Thus, the volume of one ribbon is calculated from its dimensions, and the minimum volume loaded into the crucible is as calculated from eq 2 below.

$$V_{load} = V_{ribbon} \times N = l \times w \times t \times N \quad (2)$$

Using the equation for the volume of a cylinder ($\pi r^2 h$), along with the number of wafers grown during each ribbon pull, the amount of material consumed for each ribbon pull is given by eq 3,

$$V_{consumed} = N \times n \times t \times \pi\left[\frac{d}{2}\right]^2 \quad (3)$$

The reuse volume is given by the difference between the loaded (eq 2) and consumed (eq 3) volumes.

In modeling the growth of Ga_2O_3, the target wafer diameter was 6″, or ∼150 mm, so in sticking with standard units, d = 150 mm. The ribbons were assumed to be 1 mm larger than the wafer diameter, at w = 151 mm, with the number of wafers per ribbon as n = 13 and pulling N = 16 ribbons at a time. The ribbons were pulled to a total length of 2 m. Given these parameters, the loaded (9664 cm^3), consumed (3676 cm^3), and re-used (5988 cm^3) volumes were calculated.

Among the six process steps, the reshaping/coring step was the least expensive, at around $14/wafer. Out of this cost, the labor costs are the largest portion at a little over $5/wafer, followed by the materials costs (just over $3/wafer). The material cost is driven by the coring bits necessary for cutting out the wafer shape. The energy, equipment, facilities, and maintenance cost for this step combined contribute less than $5 to the total cost of the wafer.

3.4. Grinding. Grinding is unique to EFG-grown wafers. In CZ, the boule is cut along the planes of the wafer surface, which means they are cut near the final wafer thickness. In EFG, however, it is necessary to grow the ribbon in a thickness considerably larger than the downstream-process-expected 500 μm wafer.[17,49] In the model, it is assumed that the ribbon is grown at 1.5 mm thick. The surface defects in the ribbon become the surface of the wafer, so they must be ground off. Furthermore, because of the low intrinsic thermal conductivity of gallium oxide, the final wafer thickness is desired to be as minimal as possible for optimum device performance.[50]

The grinding step involves the removal of the excess thickness, bringing the wafer down to the size before the finer lapping and polishing step. For this grinding step, the removal rate was taken at 20 μm/minute using a 600-grit grinding wheel. The thickness of the starting ribbon affects the grinding step, as a thicker ribbon will require a longer grind. When grinding the wafers, 10 μm was left over the target wafer thickness to allow for polishing to a smooth surface using lapping and a chemical mechanical polish (CMP) in the next process step. Grinding accounts for a little over $20/wafer. This cost is primarily from equipment costs (∼$10/wafer) and labor costs (∼$4/wafer). The material costs are kept relatively low in this step (<$5/wafer) by the fact that the grinding wheels have longer lifetimes, so they do not need to be replaced frequently.

3.5. Surface Preparation. At this point, after the bulk grinding procedure has been completed, the wafers grown via EFG are assumed to be essentially indistinguishable from those grown via CZ. The surface preparation step is the final step to prepare the wafer for epitaxial growth. The wafer is polished to the final desired thickness, cleaned, and inspected. Lapping and CMP together remove the final 10 μm from the wafer. There are two cleaning steps assumed necessary, with the final cleaning step occurring right before the final wafer inspection.

The material cost is around $15 and is primarily driven by the short lifetime of the lapping wheel. The equipment cost (a

https://doi.org/10.1021/acs.cgd.2c00340
Cryst. Growth Des. 2022, 22, 4854−4863

little over $5/wafer) is driven by the underutilization of the wafer cleaning and inspection stations at the projected run rate. As discussed previously, for the purpose of the model, equipment is assumed to be new and dedicated only in this process. At the assumed production rate of 5000 wafers a month, both pieces of equipment are utilized at less than 40% of their capacity. This leads to equipment costs accounting for 1/5 of the total costs in the surface preparation step. This is also causing a labor cost spike (just over $5/wafer). Labor is calculated based on the number of machines, not on machine utilization; thus, a machine utilized at 1% has the same labor cost as one utilized 100%. The total cost per wafer for the surface preparation steps is a little more than $30/wafer. Thus, this polishing, cleaning, and wafer inspection step remains unchanged from the CZ model.

3.6. Epitaxial Growth. For the heteroepitaxial growth step in the fabrication of Ga_2O_3 wafers, growth rates of over 250 μm/h have previously been achieved using halide vapor phase epitaxy (HVPE),[51] which is a chemical vapor deposition (CVD) technique in which one of the precursors is a halide. However, growing films at that rapid rate results in a rough surface of the film. HVPE typically consists of a reaction between the metal precursor (Ga in this case) and a halide to form a more chemically reactive metal halide (commonly Ga + HCl → GaCl + H_2 or a similar reaction starting from Cl_2), which is then reacted with the anion of choice in a different temperature zone (most commonly GaCl + O_2 → Ga_2O_3 + Cl_2, but sometimes using H_2O as the oxygen precursor).[51−53] Theoretical and experimental results indicate that Ga_2O_3 growth via HVPE is thermodynamically controlled and that the GaCl partial pressure plays a significant role in the growth rate. In a thermodynamic study of HVPE growth rates for Ga_2O_3, a growth rate of 20 μm/h was found to be both reasonable and achievable,[53] so 20 μm/h was set as the epitaxial growth rate in the model.

Because of the wider bandgap of Ga_2O_3, the epitaxial layer does not need to be as thick as it does, for example, for SiC. For the EFG model, a 3 μm layer was assumed to be sufficient. The previous modeling had used MOCVD to grow the epitaxy layer and had further grown it to 30 μm to compare against incumbent SiC wafers. For the epitaxial growth step, a batch size of 10 wafers was assumed. With the parameters listed above, the total cost of the epitaxial growth step was slightly over $20/wafer. The primary driver of this cost was the cost of the equipment, which accounts for a little less than $15 of that total. Maintenance of the equipment and facility came out to just under $5/wafer, which was in the same range as the total material cost. The gallium trichloride precursor accounts for most of that material cost. Labor, energy usage, and the facility each contributed less than $1/wafer. A 10× thinner layer resulted in an epitaxial growth cost that was 1/2 that reported in the previous CZ model.[2] It should be noted that the thinner epitaxial layer savings would be true with CZ growth as well; Figure 3 (left) reflects a CZ-grown wafer price with the previous, thicker, epitaxial layer.

4. DISCUSSION

4.1. Key Limitations/Changes: The Volatile Price of Iridium. The cost of iridium has a substantial effect on the projected price of Ga_2O_3 wafers. The crucible material used for Ga_2O_3 growth from the melt has to withstand a typical growth cycle: charging with precursor powder, heating to high temperatures, growing the crystal at the oxide melting point in the necessary conditions (which includes a non-negligible oxygen content), and cooling the crucible/residual charge.[31] Iridium is one of the few materials that can withstand the conditions needed for Ga_2O_3 growth. Unfortunately, iridium prices have skyrocketed over the past five years,[54] increasing by over an order of magnitude from $520/troy oz. to $5300/troy oz. between January 2016 and August 2021, hitting a peak average monthly cost of $6300/troy oz in May 2021 (Figure 4). Thus, any transition away from iridium and toward less

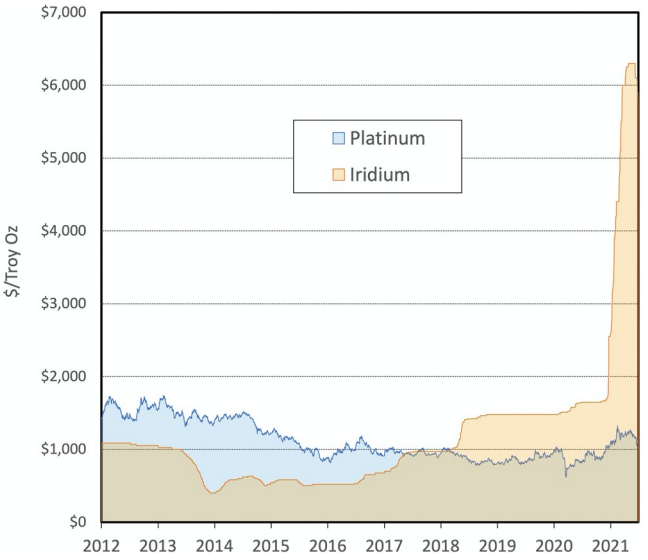

Figure 4. Iridium and platinum price fluctuations over the last 5 years.

expensive crucible materials, if feasible from an engineering standpoint, could provide a significant economic benefit in the price per wafer for Ga_2O_3.

Industrially, for high-temperature oxide growth, the most common crucible materials used are iridium, molybdenum, tungsten, or some other refractory metal. In the case of gallium oxide, the crystal needs a partial pressure of oxygen in the chamber to limit the decomposition of the molten material.[19,28] This is due to the propensity of molten Ga_2O_3 to decompose into gaseous O_2, O, Ga_2O, GaO, Ga, as well as liquid Ga, which, if left unchecked, lead to significant instabilities in growth.[20] This requirement for oxygen in the growth chamber eliminates the possibility of using tungsten or molybdenum crucibles, which would oxidize and degrade in the aforementioned oxidizing conditions.

As a rule of thumb, it is better to use metal crucibles for melt growth of oxide crystals and oxide crucibles for metallic crystal growth. However, a couple of alternatives to iridium have been used in the literature, and if feasible, these shifts could aid in reducing the cost of Ga_2O_3 wafers. The first option breaks the rule of thumb of avoiding oxide crucibles for oxide crystal growth, in which single-crystal sapphire crucibles were used for a study growing Ga_2O_3 via EFG published in 2014.[55] However, one major issue with using sapphire as the crucible material is diffusion of aluminum into Ga_2O_3, which has been observed even at lower temperatures, with both Al_2O_3 and Ga_2O_3 as solids at an interface.[56] Another crucible alternative is a 70% platinum−30% rhodium alloy, used in a 2016 study growing Ga_2O_3 in ambient air using the vertical Bridgman growth method.[22] In this method, however, the crucible then had to be destructively removed from the grown crystal. Although

https://doi.org/10.1021/acs.cgd.2c00340
Cryst. Growth Des. 2022, 22, 4854−4863

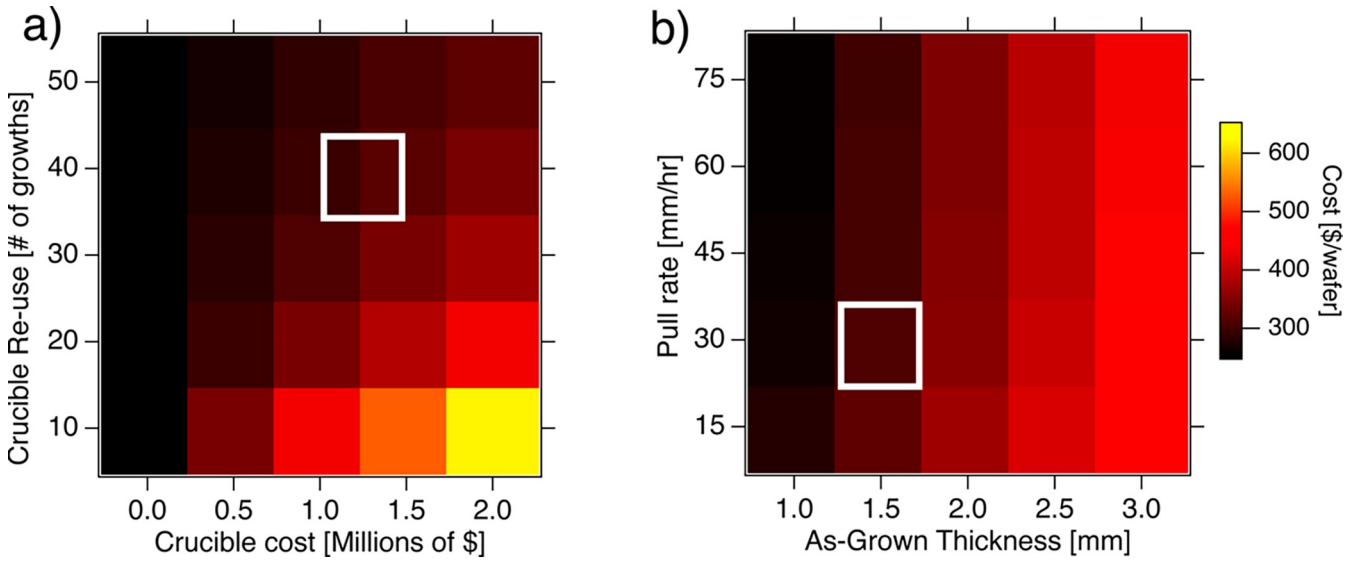

Figure 5. Cost-sensitivity analysis focused on (a) the cost of the crucible and the number of uses for each crucible, and (b) the pull thickness of the EFG ribbon and the grinding rate for the initial grind-down to approximate the final wafer thickness. White boxes indicate the parameters used for the baseline model, as reported in the previous sections.

platinum has not experienced a price increase (Figure 4), with rhodium mirroring the iridium price spike, the Pt-Rh alloy would not improve on the cost analysis even without the destructive removal process. Regardless, these studies demonstrate that alternatives have been used before, so finding a less cost-prohibitive material may be possible.

4.2. Cost-Sensitivity Analysis and Paths to Reducing Wafer Costs. We applied variations on the cost driving parameters discussed in the previous section to the EFG growth model. Specifically, the two types of parameters that were found to drive the cost significantly were those involving the crucible (Figure 5a), specifically the crucible cost and reuse, and the crystal growth step (Figure 5b), with the varying pull rate and as-grown thickness of the crystal pull. The as-grown crystal thickness directly affects the grinding time needed per wafer in the "grinding/lapping" step. In performing this cost-sensitivity analysis, we provide a road map for which parameters should be the focus, from an engineering perspective, to improve the economic viability of commercial Ga_2O_3 wafers. We provide this information as a general suggestion for moving forward, with the knowledge that other parameters may also play vital roles in the cost model.

Figure 5a shows the effects of the iridium crucible cost and the number of times the crucible is used before recycling on the total cost per wafer. Lowering the cost of the crucible (for which the range shown is $0 to $2 million, to encompass a complete range from negligible crucible price, through the current approximate cost, and beyond) significantly decreases the cost per wafer. This result is expected, given that the cost model demonstrated a significant cost driven by the crucible. The number of uses per crucible also has a significant effect on the cost per wafer, as reuse correlates directly to how often the crucible must be repurchased (while still factoring in a recycling rebate for sending the crucible back to the manufacturer).

Another avenue for decreasing the cost of wafers grown via EFG is to pull ribbons with thicknesses close to the final desired wafer thickness. As calculated in the previous section, this decreases the volume of precursor powder consumed per wafer and allows for the growth/pull rate to be increased. In turn, the reduction in thickness reduces both the grinding time and the consumption of grinding pads for those machines. The ribbon thickness and grinding rate of the initial thinning and their effects on the per-wafer cost are shown in Figure 5b. The ribbon thickness has a direct effect on the cost per wafer as well, in large part due to the additional Ga_2O_3 powder that is consumed and nonrecoverable. The cost for the Ga_2O_3 powder would be expected to decrease as Ga_2O_3 wafer production ramped up, and the powder became more of a commodity product.

5. SUMMARY AND OUTLOOK

In this study, we presented a bottom-up TEA of the prospective cost of 6″ EFG-grown Ga_2O_3 epi-wafers, including cost-comparison analysis and feasibility considerations of each process step required for volume manufacturing. With the stated assumptions, including labor, equipment, maintenance, facilities, energy, and materials, the total cost for production, at a run rate of 5000 6″ Ga_2O_3 epi-wafers per month, was calculated at around $320/wafer. A cost-sensitivity analysis of the model was performed, and parameters that most significantly impacted the overall wafer cost were the crucible cost and reuse (particularly given the sharp spike in iridium prices over the last 5 years), and to a lesser extent, the ribbon pull rate and thickness during the crystal growth step. The CZ model was adjusted to account for the significant iridium price increase and, when compared to the modified CZ model, EFG growth was found to be 2× lower in cost, given 2021 iridium pricing (~$6,000/troy ounce). Ultimately, Ga_2O_3 presents significant cost-competitive and feasibility potential over other wide bandgap semiconductors (e.g., SiC and GaN) for high-temperature and high-power electronics.

High-power and high-temperature electronics are important across a wide range of applications, from the monitoring of geothermal wells during drilling and high-temperature industrial processes to fuel cell cars and missions to Venus. High-temperature electronics enable applications where cooling is not practical or a reduced form factor is necessary,

https://doi.org/10.1021/acs.cgd.2c00340
Cryst. Growth Des. 2022, 22, 4854−4863

particularly when coupled with stability and reliability in corrosive (or other extreme) environments. While silicon (Si) took the electronics field by storm over the past several decades, Si electronics are limited to a maximum temperature of around 150 °C. High-power and high-temperature electronic technologies based on the wide bandgap semiconductors SiC and GaN have been shown to both be more efficient and expand the operational temperature range compared to their Si-based counterparts. However, these materials are significantly more expensive because of the complexity of growing substrates (GaN), hardness of the material requiring expensive consumables (SiC), and the overall less-scalable methods available for crystal growth. Thus, because of the ability to grow via melt-growth techniques such as EFG, Ga_2O_3 provides an attractive per-wafer manufacturing cost, which should enable increased deployment of high-power and high-temperature electronics while competing at an economic level with the incumbent Si and up-and-coming SiC technologies.

AUTHOR INFORMATION

Corresponding Authors

Karen N. Heinselman − *National Renewable Energy Laboratory, Golden, Colorado 80401, United States;* orcid.org/0000-0003-0287-3019; Email: Karen.Heinselman@nrel.gov

Samantha B. Reese − *National Renewable Energy Laboratory, Golden, Colorado 80401, United States;* orcid.org/0000-0002-6378-9489; Email: Samantha.Reese@nrel.gov

Authors

Drew Haven − *Saint-Gobain, Milford, New Hampshire 03055, United States*

Andriy Zakutayev − *National Renewable Energy Laboratory, Golden, Colorado 80401, United States;* orcid.org/0000-0002-3054-5525

Complete contact information is available at: https://pubs.acs.org/10.1021/acs.cgd.2c00340

Author Contributions

Conceptualization, S.B.R. and A.Z.; Investigation, K.N.H. and S.B.R.; Writing−Original Draft, K.N.H. and S.B.R.; Writing−Review and Editing, K.N.H., D.H., A.Z., and S.B.R.; Funding Acquisition, A.Z.

Funding

Office of Energy Efficiency and Renewable Energy (EERE) Advanced Manufacturing Office (AMO) under Contract No. DE-10AC36-08GO28308.

Notes

The authors declare no competing financial interest.

ACKNOWLEDGMENTS

This work was authored in part at the National Renewable Energy Laboratory (NREL), operated by Alliance for Sustainable Energy, LLC, for the U.S. Department of Energy (DOE) under Contract No. DE-10AC36-08GO28308. Funding was provided by the Office of Energy Efficiency and Renewable Energy (EERE) Advanced Manufacturing Office (AMO). The views expressed in the article do not necessarily represent the views of the DOE or the U.S. Government. The authors wish to thank Al Hicks for his work on graphically representing the EFG process and Hope Wikoff for her assistance in generating attractive plots and editing.

ABBREVIATIONS

Ga_2O_3, gallium oxide; SiC, silicon carbide; GaN, gallium nitride; EFG, edge-defined film-fed growth; CZ, Czochralski; TEA, technoeconomic analysis; PV, photovoltaic; DFMA, Design for Manufacture and Assembly; CMP, chemical mechanical polish; CVD, chemical vapor deposition; HVPE, halide vapor phase epitaxy

REFERENCES

(1) Higashiwaki, M.; Sasaki, K.; Kuramata, A.; Masui, T.; Yamakoshi, S. Development of gallium oxide power devices. *Phys. Status Solidi Appl. Mater. Sci.* **2014**, *211*, 21−26.

(2) Reese, S. B.; Remo, T.; Green, J.; Zakutayev, A. How Much Will Gallium Oxide Power Electronics Cost? *Joule* **2019**, *3*, 903−907.

(3) Pearton, S. J.; Yang, J.; Cary, P. H., IV; Ren, F.; Kim, J.; Tadjer, M. J.; Mastro, M. A. A review of Ga2O3 materials, processing, and devices. *Appl. Phys. Rev.* **2018**, *5*, No. 011301.

(4) Kotecha, R.; Metzger, W.; Mather, B.; Narumanchi, S.; Zakutayev, A. Modeling and Analysis of Gallium Oxide Vertical Transistors. *ECS J. Solid State Sci. Technol.* **2019**, *8*, Q3202−Q3205.

(5) Guo, D.; Liu, H.; Li, P.; Wu, Z.; Wang, S.; Cui, C.; Li, C.; Tang, W. Zero-power-consumption solar-blind photodetector based on β-Ga2O3/NSTO heterojunction. *ACS Appl. Mater. Interfaces* **2017**, *9*, 1619−1628.

(6) Lee, S. H.; Kim, S. B.; Moon, Y. J.; Kim, S. M.; Jung, H. J.; Seo, M. S.; Lee, K. M.; Kim, S. K.; Lee, S. W. High-Responsivity Deep-Ultraviolet-Selective Photodetectors Using Ultrathin Gallium Oxide Films. *ACS Photonics* **2017**, *4*, 2937−2943.

(7) Ahn, S.; Lin, Y. H.; Ren, F.; Oh, S.; Jung, Y.; Yang, G.; Kim, J.; Mastro, M. A.; Hite, J. K.; Eddy, C. R., Jr.; Pearton, S. J. Effect of 5 MeV proton irradiation damage on performance of β-Ga2O3 photodetectors. *J. Vac. Sci. Technol., B: Nanotechnol. Microelectron.: Mater., Process., Meas., Phenom.* **2016**, *34*, No. 041213.

(8) Oshima, T.; Okuno, T.; Fujita, S. Ga2O3 thin film growth on c-plane sapphire substrates by molecular beam epitaxy for deep-ultraviolet photodetectors. *Japanese J. Appl. Phys.* **2007**, *46*, 7217−7220.

(9) Guo, D. Y.; Wu, Z. P.; An, Y. H.; Guo, X. C.; Chu, X. L.; Sun, C. L.; Li, L. H.; Li, P. G.; Tang, W. H. Oxygen vacancy tuned Ohmic-Schottky conversion for enhanced performance in b-Ga2O3 solar-blind ultraviolet photodetectors. *Appl. Phys. Lett.* **2014**, *105*, No. 023507.

(10) Hou, C.; Gazoni, R. M.; Reeves, R. J.; Allen, M. W. Oxidized Metal Schottky Contacts on (010) β-Ga2O3. *IEEE Electron Device Lett.* **2019**, *40*, 337−340.

(11) Hou, C.; Gazoni, R. M.; Reeves, R. J.; Allen, M. W. High-Temperature β-Ga2O3 Schottky Diodes and UVC Photodetectors Using RuOx Contacts. *IEEE Electron Device Lett.* **2019**, *40*, 1587−1590.

(12) Heinselman, K.; Walker, P.; Norman, A.; Parilla, P.; Ginley, D.; Zakutayev, A. Performance and reliability of β-Ga2O3 Schottky barrier diodes at high temperature. *J. Vac. Sci. Technol., A* **2021**, *39*, No. 040402.

(13) Trinchi, A.; Wlodarski, W.; Li, Y. X. Hydrogen sensitive Ga2O3 Schottky diode sensor based on SiC. *Sens. Actuators, B* **2004**, *100*, 94−98.

(14) Wu, N.; Chen, Z.; Xu, J.; Chyu, M.; Mao, S. X. Impedancemetric Pt/YSZ/Au-Ga2O3 sensor for CO detection at high temperature. *Sens. Actuators, B* **2005**, *110*, 49−53.

(15) Reiprich, J.; Isaac, N. A.; Schlag, L.; Hopfeld, M.; Ecke, G.; Stauden, T.; Pezoldt, J.; Jacobs, H. O. Corona discharge assisted growth morphology switching of tin-doped gallium oxide for optical gas sensing applications. *Cryst. Growth Des.* **2019**, *19*, 6945−6953.

https://doi.org/10.1021/acs.cgd.2c00340
Cryst. Growth Des. 2022, 22, 4854−4863

(16) Baldini, M.; Galazka, Z.; Wagner, G. Recent progress in the growth of β-Ga2O3 for power electronics applications. *Mater. Sci. Semicond. Process.* **2018**, *78*, 132−146.
(17) Zhang, S.; Lian, X.; Ma, Y.; Liu, W.; Zhang, Y.; Xu, Y.; Cheng, H. Growth and characterization of 2-inch high quality β-Ga2O3 single crystals grown by EFG method. *J. Semicond.* **2018**, *39*, No. 083003.
(18) Aida, H.; Nishiguchi, K.; Takeda, H.; Aota, N.; Sunakawa, K.; Yaguchi, Y. Growth of β-Ga2O3 single crystals by the edge-defined, film fed growth method. *Jpn. J. Appl. Phys.* **2008**, *47*, 8506−8509.
(19) Galazka, Z.; Uecker, R.; Irmscher, K.; Albrecht, M.; Klimm, D.; Pietsch, M.; Brützam, M.; Bertram, R.; Ganschow, S.; Fornari, R. Czochralski growth and characterization of β-Ga2O3 single crystals. *Cryst. Res. Technol.* **2010**, *45*, 1229−1236.
(20) Galazka, Z.; Irmscher, K.; Uecker, R.; Bertram, R.; Pietsch, M.; Kwasniewski, A.; Naumann, M.; Schulz, T.; Schewski, R.; Klimm, D.; Bickermann, M. On the bulk β-Ga2O3 single crystals grown by the Czochralski method. *J. Cryst. Growth* **2014**, *404*, 184−191.
(21) Galazka, Z.; Uecker, R.; Klimm, D.; Irmscher, K.; Naumann, M.; Pietsch, M.; Kwasniewski, A.; Bertram, R.; Ganschow, S.; Bickermann, M. Scaling-Up of Bulk β-Ga2O3 Single Crystals by the Czochralski Method. *ECS J. Solid State Sci. Technol.* **2017**, *6*, Q3007−Q3011.
(22) Hoshikawa, K.; Ohba, E.; Kobayashi, T.; Yanagisawa, J.; Miyagawa, C.; Nakamura, Y. Growth of β-Ga2O3 single crystals using vertical Bridgman method in ambient air. *J. Cryst. Growth* **2016**, *447*, 36−41.
(23) Demina, S. E.; Kalaev, V. V. 3D unsteady computer modeling of industrial scale Ky and Cz sapphire crystal growth. *J. Cryst. Growth* **2011**, *320*, 23−27.
(24) Timofeev, V. V.; Kalaev, V. V.; Ivanov, V. G. 3D melt convection in sapphire crystal growth: Evaluation of physical properties. *Int. J. Heat Mass Transfer* **2015**, *87*, 42−48.
(25) Liu, W.; Lu, J.; Chen, H.; Yan, W.; Min, C.; Lian, Q.; Wang, Y.; Cheng, P.; Liu, C.; Xu, Y. Study on crystal-melt interface shape of sapphire crystal growth by the KY method. *J. Cryst. Growth* **2015**, *431*, 15−23.
(26) Kalaev, V.; Sattler, A.; Kadinski, L. Crystal twisting in Cz Si growth. *J. Cryst. Growth* **2015**, *413*, 12−16.
(27) Akselrod, M. S.; Bruni, F. J. Modern trends in crystal growth and new applications of sapphire. *J. Cryst. Growth* **2012**, *360*, 134−145.
(28) Tang, X.; Liu, B.; Yu, Y.; Liu, S.; Gao, B. Numerical analysis of difficulties of growing large-size bulk β-Ga2O3 single crystals with the czochralski method. *Crystals* **2021**, *11*, 25.
(29) LaBelle, H. E. Growth of controlled profile crystals from the melt: Part II - Edge-defined, film-fed growth (EFG). *Mater. Res. Bull.* **1971**, *6*, 581−589.
(30) Ciszek, T. F. Edge-defined Film-fed Growth (EFG) of Silicon Ribbons. *Mater. Res. Bull.* **1972**, *7*, 731−737.
(31) Cockayne, B. Czochralski Growth of Oxide Single Crystals: Iridium Crucibles and Their Use. *Platinum Met. Rev.* **1974**, *18*, 86−91.
(32) Ciszek, T. F., Wang, T. H., Page, M. R., Landry, M. D., Bauer, R. E. Silicon Materials Research on Growth Processes, Impurities, and Defects. *Presented at the National Center for Photovoltaics and Solar Program Review Meeting* 24-26 March 2003, Denver, Colorado.
(33) LaBelle, H. E. EFG, the invention and application to sapphire growth. *J. Cryst. Growth* **1980**, *50*, 8−17.
(34) Novak, R. E.; Metzl, R.; Dreeben, A.; Berkman, S.; Patterson, D. L. The production of EFG sapphire ribbon for heteroepitaxial silicon substrates. *J. Cryst. Growth* **1980**, *50*, 143−150.
(35) Becker, W.; Christensen, D.; Cutler, D.; Maguire, J.; McCabe, K.; Reese, S.; Speake, A. Technoeconomic Design of a Geothermal-Enabled Cold Climate Zero Energy Community. *J. Energy Resour. Technol.* **2021**, *143*, 100902.
(36) Horowitz, K., Remo, T., Reese, S., Horowitz, K., Remo, T., Reese, S. A Manufacturing Cost and Supply Chain Analysis of SiC Power Electronics Applicable to Medium-Voltage Motor Drives A Manufacturing Cost and Supply Chain Analysis of SiC Power Electronics Applicable to Medium-Voltage Motor Drives, 2017.
(37) Powell, D. M.; Winkler, M. T.; Choi, H. J.; Simmons, C. B.; Needleman, D. B.; Buonassisi, T. Crystalline silicon photovoltaics: a cost analysis framework for determining technology pathways to reach baseload electricity costs. *Energy Environ. Sci.* **2012**, *5*, 5874−5883.
(38) Ward, J. S.; Remo, T.; Horowitz, K.; Woodhouse, M.; Sopori, B.; VanSant, K.; Basore, P. Techno-economic analysis of three different substrate removal and reuse strategies for III-V solar cells. *Progr. Photovolt.: Res. Appl.* **2016**, *24*, 1284−1292.
(39) Singh, A.; Reese, S.; Akar, S. Performance and Techno-Economic Evaluation of a Three-Phase, 50-kW SiC-Based PV Inverter. In *2019 IEEE 46th Photovoltaic Specialists Conference (PVSC)*, 2019, pp. 695−701.
(40) Reese, S.; Mann, M.; Remo, T.; Horowitz, K. Regional manufacturing cost structures and supply chain considerations for medium voltage silicon carbide power applications. In *Proceedings of the ASME 2018 13th International Manufacturing Science and Engineering Conference. Volume 2: Materials; Joint MSEC-NAMRC-Manufacturing USA*. College Station, Texas, USA, 2018.
(41) Galazka, Z. Growth of bulk β-Ga2O3single crystals by the Czochralski method. *J. Appl. Phys.* **2022**, *131*, No. 031103.
(42) Miller, W.; Böttcher, K.; Galazka, Z.; Schreuer, J. Numerical modelling of the czochralski growth of β-Ga2O3. *Crystals* **2017**, *7*, 1−15.
(43) DFMA. Boothroyd Dewhurst, Inc. https://www.dfma.com.
(44) Schwabe, D.; Uecker, R.; Bernhagen, M.; Galazka, Z. An analysis of and a model for spiral growth of Czochralski-grown oxide crystals with high melting point. *J. Cryst. Growth* **2011**, *335*, 138−147.
(45) Liu, H.; Zhan, G.; Wu, G.; Song, C.; Wu, X.; Xu, Q.; Chen, X.; Hu, X.; Zhuang, N.; Chen, J. Improved Edge-Defined Film-Fed Growth of Incongruent-Melting Tb3Al5O12 Crystal with High Magneto-Optical and Thermal Performances. *Cryst. Growth Des.* **2019**, *19*, 1521−1531.
(46) Ravi, K. V. The growth of EFG silicon ribbons. *J. Cryst. Growth* **1977**, *39*, 1−16.
(47) Fu, B.; Mu, W.; Zhang, J.; Wang, X.; Zhuang, W.; Yin, Y.; Jia, Z.; Tao, X. A study on the technical improvement and the crystalline quality optimization of columnar β-Ga2O3 crystal growth by an EFG method. *CrystEngComm* **2020**, *22*, 5060−5066.
(48) Mu, W.; Jia, Z.; Yin, Y.; Fu, B.; Zhang, J.; Zhang, J.; Tao, X. Solid-liquid interface optimization and properties of ultra-wide bandgap β-Ga2O3 grown by Czochralski and EFG methods. *CrystEngComm* **2019**, *21*, 2762−2767.
(49) Schmidt, W.; Woesten, B.; Kalejs, J. P. Manufacturing technology for ribbon silicon (EFG) wafers and solar cells. *Progr. Photovolt.: Res. Appl.* **2002**, *10*, 129−140.
(50) Yuan, C.; Zhang, Y.; Montgomery, R.; Kim, S.; Shi, J.; Mauze, A.; Itoh, T.; Speck, J. S.; Graham, S. Modeling and analysis for thermal management in gallium oxide field-effect transistors. *J. Appl. Phys.* **2020**, *127*, 154502.
(51) Xiu, X.; Zhang, L.; Li, Y.; Xiong, Z.; Zhang, R.; Zheng, Y. Application of halide vapor phase epitaxy for the growth of ultra-wide band gap Ga2O3. *J. Semicond.* **2019**, *40*, No. 011805.
(52) Murakami, H.; Nomura, K.; Goto, K.; Sasaki, K.; Kawara, K.; Thieu, Q. T.; Togashi, R.; Kumagai, Y.; Higashiwaki, M.; Kuramata, A.; Yamakoshi, S.; Monemar, B.; Koukitu, A. Homoepitaxial growth of β-Ga2O3 layers by halide vapor phase epitaxy. *Appl. Phys. Express* **2015**, *8*, No. 015503.
(53) Nomura, K.; Goto, K.; Togashi, R.; Murakami, H.; Kumagai, Y.; Kuramata, A.; Yamakoshi, S.; Koukitu, A. Thermodynamic study of β-Ga2O3 growth by halide vapor phase epitaxy. *J. Cryst. Growth* **2014**, *405*, 19−22.
(54) Price Charts - PMM. http://www.platinum.matthey.com/prices/price-charts (accessed Aug. 31, 2021).
(55) Maslov, V. N.; Krymov, V. M.; Blashenkov, M. N.; Golovatenko, A. A.; Nikolaev, V. I. β-Ga2O3 crystal growing from its own melt. *Tech. Phys. Lett.* **2014**, *40*, 303−305.
(56) Goyal, A.; Yadav, B. S.; Thakur, O. P.; Kapoor, A. K.; Muralidharan, R. Effect of annealing on β-Ga2O3 film grown by

https://doi.org/10.1021/acs.cgd.2c00340
Cryst. Growth Des. 2022, 22, 4854−4863

pulsed laser deposition technique. *J. Alloys Compd.* **2014**, *583*, 214–219.

https://doi.org/10.1021/acs.cgd.2c00340
Cryst. Growth Des. 2022, 22, 4854–4863